Nuclear Engineering and Design 315 (2017) 1–10

Contents lists available at ScienceDirect

Nuclear Engineering and Design

journal homepage: www.elsevier.com/locate/nucengdes

Inclusion of models to describe severe accident conditions in the fuel simulation code DIONISIO

Martín Lemes [a], Alejandro Soba [a], Hernando Daverio [b], Alicia Denis [a,*]

[a] Sección Códigos y Modelos, Gerencia Ciclo del Combustible Nuclear, Comisión Nacional de Energía Atómica, Avenida General Paz 1499, 1650 San Martín, Provincia de Buenos Aires, Argentina

[b] Gerencia Reactores y Centrales Nucleares, Comisión Nacional de Energía Atómica, Avenida General Paz 1499, 1650 San Martín, Provincia de Buenos Aires, Argentina

ARTICLE INFO

Article history:
Received 17 October 2016
Received in revised form 8 February 2017
Accepted 11 February 2017
Available online 24 February 2017

Keywords:
LOCA
Thermal-hydraulic boundary conditions

ABSTRACT

The simulation of fuel rod behavior is a complex task that demands not only accurate models to describe the numerous phenomena occurring in the pellet, cladding and internal rod atmosphere but also an adequate interconnection between them. In the last years several models have been incorporated to the DIONISIO code with the purpose of increasing its precision and reliability. After the regrettable events at Fukushima, the need for codes capable of simulating nuclear fuels under accident conditions has come forth. Heat removal occurs in a quite different way than during normal operation and this fact determines a completely new set of conditions for the fuel materials. A detailed description of the different regimes the coolant may exhibit in such a wide variety of scenarios requires a thermal-hydraulic formulation not suitable to be included in a fuel performance code. Moreover, there exist a number of reliable and famous codes that perform this task. Nevertheless, and keeping in mind the purpose of building a code focused on the fuel behavior, a subroutine was developed for the DIONISIO code that performs a simplified analysis of the coolant in a PWR, restricted to the more representative situations and provides to the fuel simulation the boundary conditions necessary to reproduce accidental situations. In the present work this subroutine is described and the results of different comparisons with experimental data and with thermal-hydraulic codes are offered. It is verified that, in spite of its comparative simplicity, the predictions of this module of DIONISIO do not differ significantly from those of the specific, complex codes.

1. Introduction

In recent years the DIONISIO code has undergone several improvements aimed at extending its application range and increasing its predicting capacity. The modifications introduced in the 2.0 version of DIONISIO have been described in detail in previous papers (Soba and Denis, 2015; Soba et al., 2013, 2015, 2014); the main characteristics are summarized here.

An acceptable prediction of the high burnup behavior is achieved with a simplified scheme embedded in the program, where the balance equations are restricted to the most relevant isotopes involved in the fission process and the energy spectrum is reduced to one-group. Hence, the effective cross sections of these isotopes, their concentration, the power density and burnup are obtained as functions of the radial position in the pellet, average burnup, and initial enrichment in ^{235}U. Moreover, some mathematical expressions were developed to describe the behavior and progress of porosity and grain size at the very high local burnup values that can be reached at the pellet external ring.

To take into consideration the axial variation of reactor linear power and coolant temperature, the rod is divided into a user defined number of segments, as shown in Fig. 1a. All the pellets in a given segment are assumed to behave identically (subjected to identical boundary conditions). Therefore, only one pellet and the corresponding gap and cladding portions have to be simulated in each segment. Axial symmetry and also symmetry with respect to the transversal mid-plane of the pellet are assumed, as schematically shown in Fig. 1b. For this reason, a two-dimensional domain, as shown in Fig. 1c, involving the radial and axial coordinates needs to be considered. The finite elements method is used to solve the different aspects of the problem.

In every time step and for each axial section, a complete description of the local system variables is obtained by solving the tightly-coupled, non-linear differential equations describing the thermal and mechanical parameters. Then, the temperature and stress-strain distributions in the complete rod are obtained as step-like functions of the axial coordinate. With respect to the

* Corresponding author.

http://dx.doi.org/10.1016/j.nucengdes.2017.02.015
0029-5493/

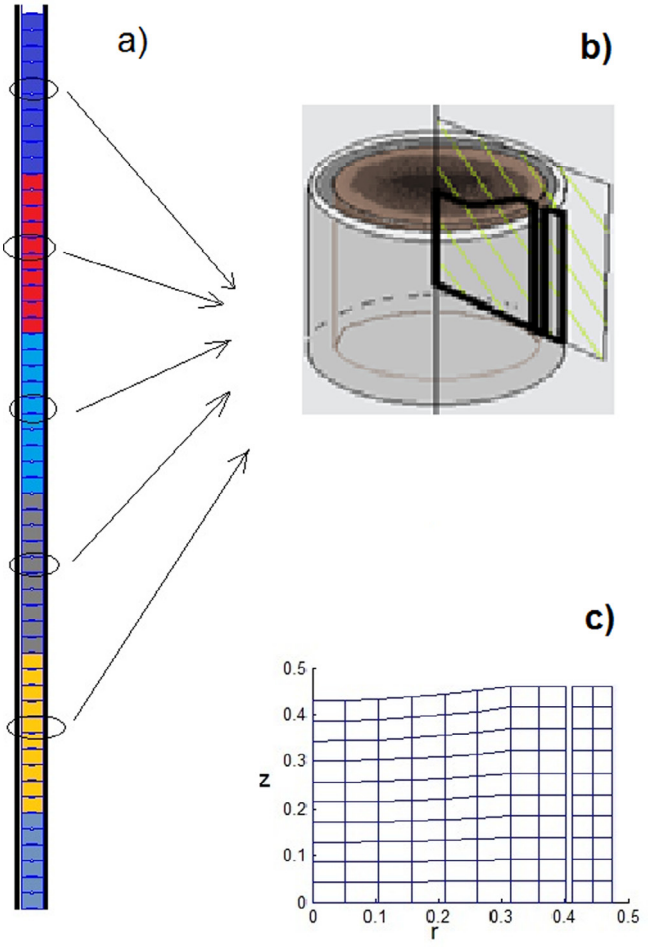

Fig. 1. a) Portion of the rod formed by several segments, each one containing a number of pellets. b) One pellet and the corresponding portions of gap and cladding; superimposed is the calculation domain. c) Finite elements discretization of the domain.

gas inventory, the code evaluates the amount of gas released by each rod segment and then that released by the whole rod. The composition of the gas mixture in the gap and its thermal conductivity are recalculated in every time step. The internal rod pressure is evaluated with the ideal gas law using the total number of gas atoms in the free volume within the rod and the average temperature in the total void volume in the rod (gap and dishings in all the segments, and plenum). The elongation of every individual pellet and the corresponding cladding are added up to obtain the total elongation of the pellet stack and the rod.

This code version has been employed so far to simulate a considerable number of experiments involving fuel rods of diverse types, operating in normal conditions. Moreover, some 380 fuel rods irradiated up to average burnup levels of 40–60 MW d/kg U, which may represent local burnup levels higher than about 200 MW d/kg U in the pellet external rim were simulated with satisfactory results.

The need of expanding the application range of the code to conditions typical of Loss of Coolant Accidents (LOCA) has prompted the development of a new module able to reproduce the thermal-hydraulic conditions in the coolant. This module is intended to give account of the numerous parameters that govern the heat exchange between the fuel rod and the coolant in accident situations, thus providing the boundary conditions necessary to simulate the fuel rod behavior during a fast excursion, particularly in such a determinant aspect as the thermal behavior.

The code simulates a vertical channel containing one fuel rod. Scenarios like forced single-phase (water or vapor) convection or double-phase flow, including departure from nucleate boiling (DNB) are taken into consideration. The model adopted analyzes and quantifies the coolant behavior in terms of the system pressure and coolant velocity. Moreover, models to describe mechanical problems occurring in accidental situations, like ballooning and burst, are also included.

In the present work a separate testing plan was first followed, which consisted in comparing the predictions of the new thermal-hydraulic module with specific codes in different flow regimes. Then it was included as a subroutine of the DIONISIO code and its results were compared with available experimental data. It is seen that the predictive ability of the general code has improved with the introduction of the heat transfer coefficients corresponding to the different patterns that can be encountered in the coolant flow.

2. Models and parameters involved

2.1. Mechanical aspects

The simulation of off-normal operation conditions imposes the need of incorporating diverse mechanical models to the code, specific for these conditions. At the present time, a model to predict clad failure (burst stress) and its localization, and another of cladding creep to evaluate clad ballooning have been recently included in the code. These subroutines are turned on if accidental conditions are met.

Cladding failure is assumed to occur when the hoop stress exceeds the burst stress, σ_B. The empirical correlation (Rosinger, 1984; Manngard et al., 2011)

$$\sigma_B = C_1 \exp(-C_2 T) \exp\left(-(C_0 W_{fO})^2\right) \quad (1)$$

was adopted as cladding burst criterion, where C_0, C_1 and C_2 are constants whose values for Zircaloy (Zry) in the single-phase domains α and β are listed in Table 1, T is the absolute temperature and W_{fO} is the total weight fraction of oxygen picked up in high temperature metal-water reactions.

For the effective cladding creep rate the correlation (Manngard et al., 2011)

$$\frac{d\varepsilon}{dt} = C_3 \exp\left(-\frac{C_4}{T}\right) \exp\left(-C_5 w_{fO}\right) \sigma_{VM}^n \quad (2)$$

was adopted. It is valid when the cladding material is in the pure α or β phase; w_{fO} is the excess oxygen weight fraction in the cladding metal layer and σ_{VM} is the von Mises stress. The constants C_3, C_4, C_5 and n adopt the values listed in Table 1 when the Zry cladding material is in the single phase domains (α or β). For the two-phase (α + β) region, the creep rate is calculated as an average of both single-phase rates weighed with the volume fractions of both phases.

Table 1
Values of the constants used in correlations (1) and (2), in pure α or β phases.

	Pure α-Zr	Pure β-Zr
C_0	1052.63	1052.63
C_1 (N cm^{-2})	8.3×10^4	2.3×10^5
C_2 (K^{-1})	0.001	0.003
C_3 (s^{-1} N^{-n} cm^{2n})	1.4523×10^{-8}	2.1751×10^{-7}
C_4 (K)	38487.0	17079.0
C_5	342.0	0.0
n	5.89	3.78

2.2. Calculation of the temperature distribution in the fuel rod

The temperature distribution in each axial segment of the fuel-cladding system is solved in DIONISIO by means of the heat exchange equation in cylindrical symmetry, which general expression is:

$$\frac{1}{r}\frac{\partial}{\partial r}\left(\kappa_r^j(T)\frac{\partial T}{\partial r}\right)+\frac{\partial}{\partial z}\left(\kappa_z^j(T)\frac{\partial T}{\partial z}\right)=-Q^j(r)+c_p^j\rho^j\frac{\partial T}{\partial t} \tag{3}$$

where T [K] is the absolute temperature; κ^j [W/(m K)] is the thermal conductivity of component j, with j = pellet, gap or cladding; the subscripts r and z indicate the possibility of non isotropic conductivity; c_p^j [J/(kg K)] is the specific heat and ρ^j [kg/m^3] is the density of component j. The heat sources considered in the independent term Q^j [W/m^3] are

$$Q^j=\begin{cases}\text{fissions and radioactive decay} & \text{for } j=\text{pellet}\\ 0 & \text{for } j=\text{gap}\\ \text{oxidation} & \text{for } j=\text{cladding}\end{cases} \tag{4}$$

For j = pellet, the thermal power density axial profile is described by different laws before and after shutdown.

$$Q^{pellet}(Z,t)=\begin{cases}Q_M(t)\cos\frac{\pi Z}{l_e} & \text{for } t\leqslant t_0\\ 6.48\times10^{-3}Q^{pellet}(Z,t_0)\left[(t-t_0)^{-0.2}-t^{-0.2}\right] & \text{for } t>t_0\end{cases} \tag{5}$$

where t_0 is the instant when shutdown takes place, l_e is the *extrapolated rod length*, Z is the axial coordinate in the rod with Z = 0 at the rod mid-length, $Q_M(t)$ is the maximum power density, which value is determined by the reactor power history. The first row of Eq. (5) represents the power density generated by the fission reactions and the second one is the contribution of the β and γ radioactive decay processes, the only heat sources after reactor shutdown (Ragheb, 2011). The rod segmentation described in Section 1 leads to the local power condition in each axial sector.

In each pellet heat removal is assumed to occur only in the radial direction, i.e.

$$\left.\frac{\partial T(r,z)}{\partial z}\right|_{z=z_{pts}}=0 \tag{6}$$

where r and z are the local radial and axial coordinates in a pellet, with $z=z_{pts}$ indicating the pellet transversal surface.

The assumption of cylindrical symmetry leads to

$$\left.\frac{\partial T(r,z)}{\partial r}\right|_{r=0}=0 \tag{7}$$

The heat removal rate through the cladding wall depends on the thermal-hydraulic conditions of the coolant and satisfies the expression

$$q''=\frac{H}{2\pi r_{ec}L}=h^{eff}[T(r_{ec})-T_{cool}] \tag{8}$$

where q'' [W/m^2] indicates the heat flux through the cladding surface, r_{ec} is the external cladding radius below the oxide layer, L is the rod length and T_{cool} [K] is the coolant bulk temperature.

H [W] is the thermal power generated in the rod which has two sources: $H=H_1+H_2$. The first one is that produced in the pellet: $H_1=Q^{pellet}(Z,t)\pi r_p^2L$, according to (5) (either by fissions or by radioactive decay), where r_p is the pellet radius. The second one, H_2, is that produced by cladding oxidation that generates 6.45×10^6 J per kg of Zr reacted with steam to give ZrO_2. The weight fractions of Zr and O in this compound are 0.74 and 0.26 respectively. Then, $H_2=6.45\times10^6\times(0.74/0.26)\times2\pi r_{ec}L\times(\Delta W/\Delta t)$, where ΔW represents the weight increase per unit cladding area due to Oxygen uptake during a time interval Δt. H and T_{cool} are assumed constant in each axial segment into which the rod is divided. From Eq. (8) $T(r_{ec})$ [K] is found.

The heat conductance between the metallic cladding surface and the coolant is expressed in this model by means of a coefficient h^{eff} [W/(m K)] that deserves special attention. It is due to two contributions acting in series: that of the oxide layer and that of the coolant. The oxide layer, despite of its small thickness represents a thermal barrier that cannot be neglected. But it is precisely due to its thickness (which is initially actually zero) that this layer cannot be given the same numerical treatment as the more bulky phases, since convergence problems would arise in the finite elements calculation. For this reason it is preferred in this work to represent the thermal effect of this layer by means of its conductance: $h^{ox}=\kappa^{oxide}/\delta^{oxide}$ where δ^{oxide} is the oxide layer thickness whose growth rate is analyzed in Section 2.4. For the thermal conductivity of the oxide, κ^{oxide}, the empirical expression given in MATPRO Version 11 (1979) is adopted.

The second contribution to h^{eff} is that due to the coolant. This is a crucial parameter since it represents the different heat removal regimes that can be encountered, either in normal operation or in accident conditions. It is precisely the analysis of this parameter, particularly in the latter type of situations, the reason of the development of the present work. These considerations are presented in Section 2.3.

Eqs. (6)–(8) express the boundary conditions of the problem which, together with the continuous matching of the solutions of (3) corresponding to the component phases, yield the temperature profile in the domain represented in Fig. 1b. To obtain these solutions, the thermal parameters of each phase need to be known.

For the pellet and cladding conductivity, the empirical expressions presented in Delete and Charles (1997), Fink and Leibowitz (1995) are used. As for the gap, the treatment including pellet cladding contact between rough surfaces and gas mixing presented in Soba and Denis (2008) was employed.

2.3. Thermal-hydraulic conditions

2.3.1. Flow regimes and heat transfer ranges

Different possible heat transfer conditions and coolant flow patterns can arise along the axis of a PWR channel in a large and intermediate break LOCA (International Agreement Report, 1986; Mochizuki, 2009; Odar, 2001). They are schematically shown in Fig. 2a. An experimental image corresponding to an electrically heated rod is also shown in Fig. 2b where the different coolant flow regimes and heat transfer modes can be appreciated (Todreas and Kazimi, 1990).

In steady-state conditions and also in the first phase of a LOCA, heat removal is carried out by *forced convection* of a single-phase turbulent flow of liquid water.

In the *subcooled nucleate boiling* region the mean water temperature is slightly below and the wall temperature is a little above the saturation temperature. The liquid immediately adjoining the hot wall is overheated giving rise to nucleation of water vapor bubbles on the wall. In this stream pattern, which is described as *bubbly flow*, the water flow breaks the bubbles off the wall provoking the rupture of the boundary layer; the flow changes from laminar to turbulent thus enhancing the heat removal from the rod while the bubbles condense in the subcooled liquid region (Manngard et al., 2011).

When the saturation temperature is reached in the whole channel, the heat removal regime is described as *nucleate boiling*. The bubbles continuously created on the cladding wall migrate towards the bulk but do not condense any longer. They coalesce giving rise to a pattern which is described as *slug flow*. These large

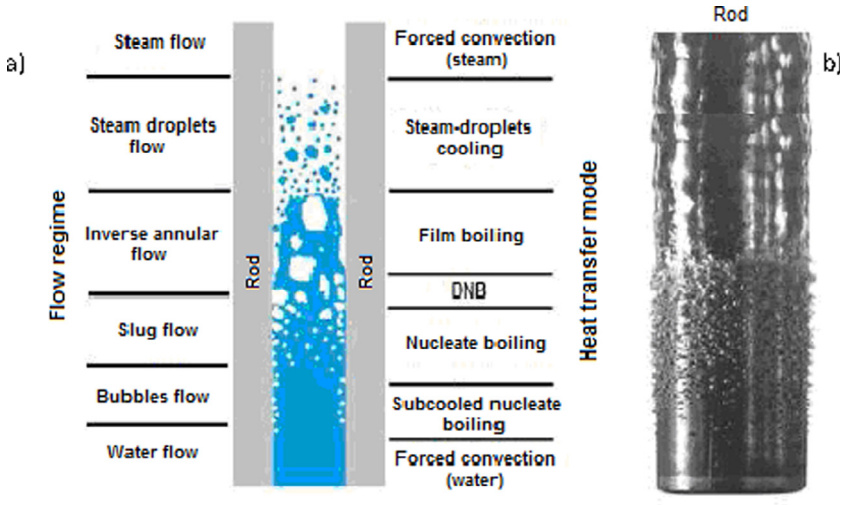

Fig. 2. a) Heat transfer an flow configurations with high heat flux (International Agreement Report, 1986); b) image of the distribution of convective boiling around a heated rod (Todreas and Kazimi, 1990).

bubbles provoke displacement of water from the channel center towards the layers closer to the cladding. Heat transfer in this region is still quite efficient (Manngard et al., 2011).

The maximum heat flux that can be removed is called *critical heat flux* (CHF). It represents the thermal limit at which the boiling regime changes during heating. At this point the vapor bubbles abruptly form a film on the heating surface that thermally insulates the heater from the liquid (Collier and Thome, 1994). If the generated heat flux exceeds this level, the heated surface can no longer hold the contact with the liquid and a boiling crisis occurs, associated with a drastic decrease of the heat transfer coefficient (Chen, 2012). The transition from *nucleate boiling* to *film boiling* is characterized by the change from bubbles or slug flow to *inverse annular flow*. Due to the high heat flux density, the liquid water detaches from the cladding wall giving rise to the formation of a thin vapor layer next to the wall, through which the heat has to be removed by conduction. This phenomenon is described as *departure from nucleate boiling* (DNB).

For heat flux values higher than the CHF, a *steam-droplets* (mist) *flow* is established. In an even higher heat flux range, the droplets are finally evaporated in the channel center. The heat transfer coefficient shows a sudden decrease also in this region. The vapor is overheated due to continuous heat addition and pressure decrease. The flow pattern in this range is turbulent vapor.

2.3.2. Calculation of the critical heat flux

The CHF is a major limit for reactor safety since if the heat flux through the cladding is higher than this value, the cladding wall temperature will rapidly increase. A number of empirical correlations and physical models have been proposed during the past decades to calculate the CHF in terms of the mass flow, pressure, temperature, working power, as well as the fuel element geometry, mainly the hydraulic diameter. The adoption in several recent works of a table of CHF values is based on its higher accuracy and more extended range of application (Chen, 2012).

Nevertheless, in this work the Bowring correlation (Todreas and Kazimi, 1990)

$$q''_{cr} = \frac{A - Bh_{fg}X_t}{C} \tag{9}$$

is used to determine the CHF, indicated as q''_{cr} [W/m^2]. It is given in terms of the latent heat of vaporization (h_{fg} [J/(kg K)]) and the mass fraction of vapor in the coolant (X_t); the parameters A, B and C are expressed in terms of the hydraulic diameter, the mass flow through the channel (G [kg/(m^2 s)]) and the system pressure. X_t is obtained with the Levy correlation (Levy, 1967) in terms of the equilibrium mass fraction, the fraction of subcooled vapor, the enthalpies of the coolant and the saturated liquid, the temperatures of the coolant and the cladding and the specific heat of the liquid.

For $G > 271$ kg/(m^2 s) or voids fraction higher than 80%, q''_{cr} is calculated with the Zuber correlation (FRAPTRAN 1.4, 2011),

$$q''_{cr} = 743F_gF_{sub}h_{fg}\sqrt{\rho_g}\left[\sigma \cdot g \cdot (\rho_f - \rho_g)\right]^{0.25} \tag{10}$$

in terms of the densities of liquid and vapor ($\rho_{f,g}$ [kg/m^3]); F_g and F_{sub} are correction factors for the extended void fraction range and for bulk subcooloed fluid conditions, respectively, and g is the acceleration of gravity.

Additionally, the code evaluates the *departure from nucleate boiling ratio*. This parameter, briefly indicated as DNBR, is the ratio of the heat flux needed to cause departure from nucleate to the actual local heat flux of a fuel rod. A high value of DNBR reveals a wide safety range, i.e. it indicates that in the working conditions the CHF is not reached.

2.3.3. Calculation of the heat transfer coefficient

The models generally used to predict the heat transfer coefficient quantify the rate of energy exchange between the solid surface and the fluid under different conditions. The present work assumes that the subcooled flow regime can be divided into the following steps:

i. Forced single-phase convection - Subcooled boiling.
ii. Saturated nucleate boiling.
iii. Post-critical transition boiling
iv. Post-critical film boiling
v. Forced single-phase convection to superheated vapor

Additional modes can be encountered in severe transients which are also described in the literature. Nevertheless, since the objective of DIONISIO is the simulation of the fuel behavior, the thermal-hydraulic analysis included in it is restricted to the five modes listed above.

In the nucleate boiling regime, the Thom correlation (Levy, 1967; Tong and Weisman, 1966) expresses the heat flux as the sum of two terms, one giving the contribution of nucleate boiling and the other of single phase convection.

In the post-critical zone, heat is transferred through the film formed between the cladding and the coolant. The correlation proposed by Miropolskij (International Agreement Report, 1986; Kolev, 2005) is used in this work to represent this regime.

The transition between nucleate boiling and film boiling is expressed by a coefficient represented in Fig. 3 obtained in the present work as an average between the nucleate and film boiling coefficients in the transition range, following the criterion proposed by Ramu and Weisman (1977). The fluid temperature is assumed to be higher than the saturation temperature and the fluid is assumed a single phase vapor.

2.4. High temperature oxide growth

In normal operation conditions, in which the coolant temperature is in the range 250 –400 °C, the Zircaloy cladding material exists in hexagonal close packed (hcp) structure, which contains interstitial Oxygen. It is usually indicated as α-Zr(O) phase. As stated by the model developed in MATPRO Version 11 (1979) the oxide (ZrO_2) layer that develops on the external surface grows according to different rate laws, depending on the layer thickness. The change is assumed to be due to the morphological modification that takes place in the oxide layer when it thickens. Within that model, the transition thickness, δ^{trans}, is given by a temperature dependent, Arrhenius-type expression.

For pre-transition layers, the oxide is assumed to grow according to a cubic rate law, i.e. the increase of the oxide thickness, $\Delta\delta^{ox}$, experienced during the time interval Δt is proportional to $(\Delta t)^{1/3}$. Instead, for $\delta > \delta^{trans}$, a linear law is assumed for the growth rate, i.e. $\Delta\delta^{ox}$ is proportional to Δt.

In the high temperature range, $T > 900$ °C, achievable in accident conditions, the Cathcart-Pawel (Cathcart et al., 1977) model is accepted. It assumes a parabolic rate law for the oxide layer growth, i.e. $\Delta\delta^{ox}$ proportional to $(\Delta t)^{1/2}$.

For the intermediate temperature range, an interpolation formula is adopted in the present work.

2.5. Heat transfer models coupling

The code performs an iterative procedure to select the transfer mode in each axial rod segment. As a starting step, certain coolant temperature, pressure and flow conditions are assumed for the whole rod. Then the temperature distribution in the rod and the thermal-hydraulic parameters are reevaluated. In this way the system selects the actual heat transfer coefficient operating in each axial segment and the temperature profile is recalculated.

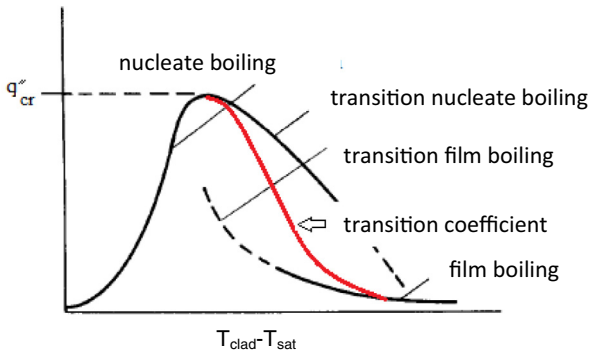

Fig. 3. Heat flux vs. overheating for different transfer regimes.

3. Results

The thermal-hydraulic module was subjected to a number of examinations. To start with, separate ideal tests were performed imposing different sets of conditions typical of accident situations. An example of this is presented in Section 3.1. After acceptance of this module, it was included as a subroutine of DIONISIO. Then, the code was run firstly in normal operation conditions and its thermal-hydraulic predictions were compared with those of the COBRA-IV code. These results are presented in Section 3.2. Then, the predictions of DIONISIO were compared with available experimental data obtained in accidental conditions. Those shown in Section 3.3 correspond to examples of the IFA series. Finally, in Section 3.4 the comparison is made with data collected in the PMK-2 facility and also with simulations carried out for these cases with the thermal-hydraulic codes RELAP5 Mod 3.1 and ATHLET Mod 1.1 Cycle A.

3.1. Analysis of a hypothetical LOCA

To perform this issue a fuel rod is assumed to have operated during 1 year at a constant linear power of 300 W/cm with a system pressure of 15.5 MPa and the coolant flowing at 5 m/s and 280 °C at the inlet. A hypothetical accident is postulated in which the pressure decreases and the coolant velocity is assumed to drop at a rate of -0.9 m/s^2; the scram is assumed to occur 1.6 s after accident initiation (when the pressure is 14.2 MPa). Two safety systems (HPIS and LPIS) are activated to provoke the discharge of water accumulators. Finally, safe conditions are reestablished with a system pressure of 1 MPa and the coolant flowing at 0.01 m/s.

For the simulation the rod is divided into 10 axial segments. In each of them the problems described in Section 2 are solved according to the local temperature and linear power conditions.

Fig. 4a shows the coolant mass flow and pressure progression in this hypothetical experiment. The initial mass flow drop provokes the accident initiation. The axial segments 5, 7 and 9 were selected to show in Fig. 4b the rod surface temperature evolution after accident initiation; a magnification of the first 10 s is shown in Fig. 4c. The effects of the initial flow drop and of the opening of the safety valves are clearly visible.

The initial time interval after accident commencement is crucial due to the large amount of heat accumulated and its slow dissipation, resulting in a considerable increase in cladding temperature. One of the safety parameters establishes a limit of 1200 °C for the cladding temperature; for higher temperatures the cladding suffers plastic deformation and oxidation is significantly enhanced. These processes, along with Hydrogen capture promote cladding embrittlement with the consequent risk of fracture.

Different fluid conditions are encountered along the fuel rod. The code evaluates the variables at each rod section following the procedure explained in Section 2.5 and determines which is the heat transfer mechanism operating in each one of the ten axial sections into which the rod is divided. Fig. 5 shows the heat transfer coefficients corresponding to the five modes considered in the present analysis; the superimposed bold line indicates which is the mode operating in each one. In the present example, heat removal is accomplished by liquid water in the six lower segments and by vapor in the upper ones.

3.2. Comparison with predictions of COBRA-IV

Before code testing in accidental scenarios, the capabilities of the thermal-hydraulic routines incorporated to DIONISIO were examined in normal operation conditions. To this end, some ideal experiments were designed and the predictions of DIONISIO were

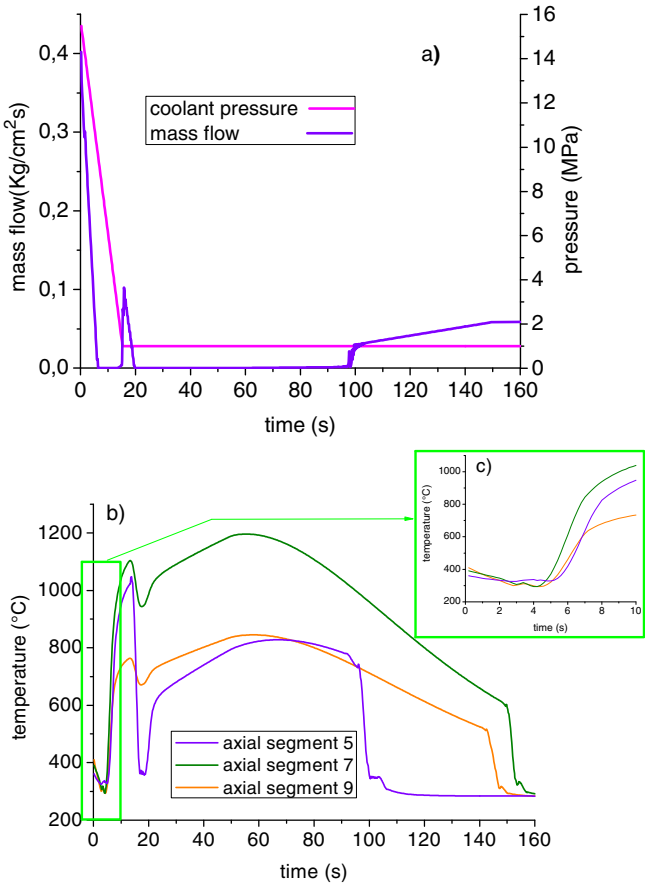

Fig. 4. a) Evolution of the coolant mass flow and pressure; b) Evolution of the rod surface temperature for selected axial segments; c) magnification of the initial interval of b).

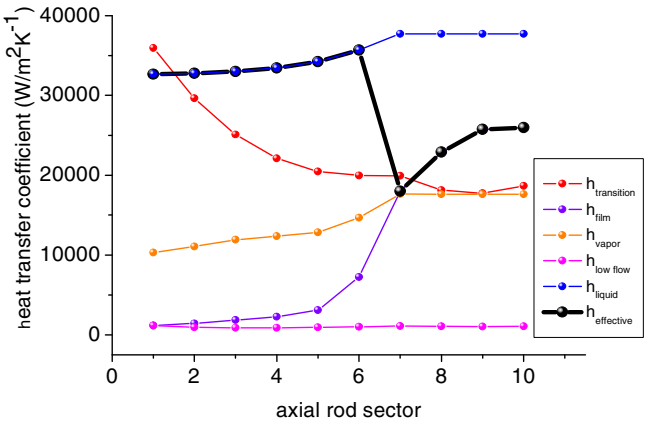

Fig. 5. Heat transfer coefficients corresponding to the five modes considered in the present analysis, according to the physical conditions operating in the ten axial rod sections.

compared with those of COBRA-IV. This is a nuclear reactor thermal-hydraulic computer code for two-phase flow analysis, especially adequate for the simulation of normal operation conditions (Webb, 1988).

Three examples are considered: 1) an ideal single rod in a channel, parameterized for the COBRA-IV simulation with 6 subchannels; a uniform linear power of 540 W/cm is assumed in the 40 cm long rod, with a coolant flow of 1 kg/s; the external rod temperature at the inlet is 290 °C and the pressure is 1150 N/cm^2; 2) an ideal device consisting of a single channel with three fuel rods, parameterized with 15 subchannels; the conditions are the same as in case 1; and 3) a fuel bundle of 37 rods, parameterized with 60 subchannels; a linear power of 500 W/cm with a peak factor of 1.1 is assumed in rods of 300 cm in length; the external rod temperature at the inlet is 260 °C and the pressure is 1100 N/cm^2.

Fig. 6 displays the comparison for four representative parameters: coolant and cladding temperature, heat flux and heat transfer coefficient between the cladding and the coolant. The rod length has been normalized in order to make the comparison clearer. The static output of COBRA-IV is considered; for the cases of 3 and 37 rods, an average channel is assumed for making the comparison with DIONISIO.

It can be observed in Fig. 6 that the greater discrepancy in the coolant temperature is obtained in the 37 rods test for which the prediction of DIONISIO is lower than that of COBRA-IV, particularly in the upper rod segment. Nevertheless, even in the worse condition, the difference between both is only about 4% in °C. As for the cladding temperature, also in °C, the estimation of DIONISIO is 5% higher than that of COBRA-IV at the lower rod segment, where the greater discrepancy is observed. Generally speaking, the single channel approximation adopted in DIONISIO, although involving a considerable simplification in the thermal-hydraulic description, compares acceptably well with such a robust specific code like COBRA-IV in the simulation of normal operation conditions.

3.3. Comparison with data of the IFA 650-1 and -2 experiments

The IFA (Instrumented Fuel Assembly) experiments were designed with the main objective of re-examining the traditional safety criteria for LOCA accidents, developed on the basis of experiments performed in the 70′. New fuel designs and cladding materials as well as a tendency to burnup extension determined the necessity of adequate measurements. The IFA tests were integral in-pile experiments under simulated LOCA conditions that included strong pressure drop and low coolant flow, designed to evaluate thermo-physical and thermo-chemical aspects like cladding temperature, ballooning, relocation of the fragmented pellet, cladding hydriding and oxidation. They were carried out in the Halden Reactor (Norway), in particular the 650-1 test in May 2003 and 650-2 in May 2004, employing instrumented segments of fresh fuel rods. The main purpose of the first experiment was to qualify the rig and its instrumentation and that of the second one, to acquire experience with a test case where ballooning and fuel failure take place, all of this before performing the subsequent experiments of the IFA 650 series that used fuel rods which had been irradiated in commercial PWR or BWR reactors reaching intermediate or high burnup.

In the IFA 650-1 and -2 tests a rod is electrically heated in a heavy water, high pressure loop. The rod length is 50 cm, its external diameter is 9.5 mm, the Zry-4 cladding wall is 0.57 mm thick and contains UO_2 pellets. Both experiments differ mainly in the base irradiation histories, the filling pressure of He (2 bar and 40 bar, respectively), the thermocouples location and the rate of pressure and coolant mass flow drop (Lestinen et al., 2003; Lestinen, 2004; Ek, 2005).

The thermal hydraulic model described in the present work was applied to simulate the experimental conditions of both tests. Power history, geometric rod characteristics like pellet and cladding radii, rod length and hydraulic aspects like coolant flow, pressure and temperature at the inlet are given as inputs for the simulation.

In experiment IFA 650-1 the linear power suffered stepwise variations followed by periods of constant power. In the meantime, six pressure drops followed by stationary periods took place. Ther-

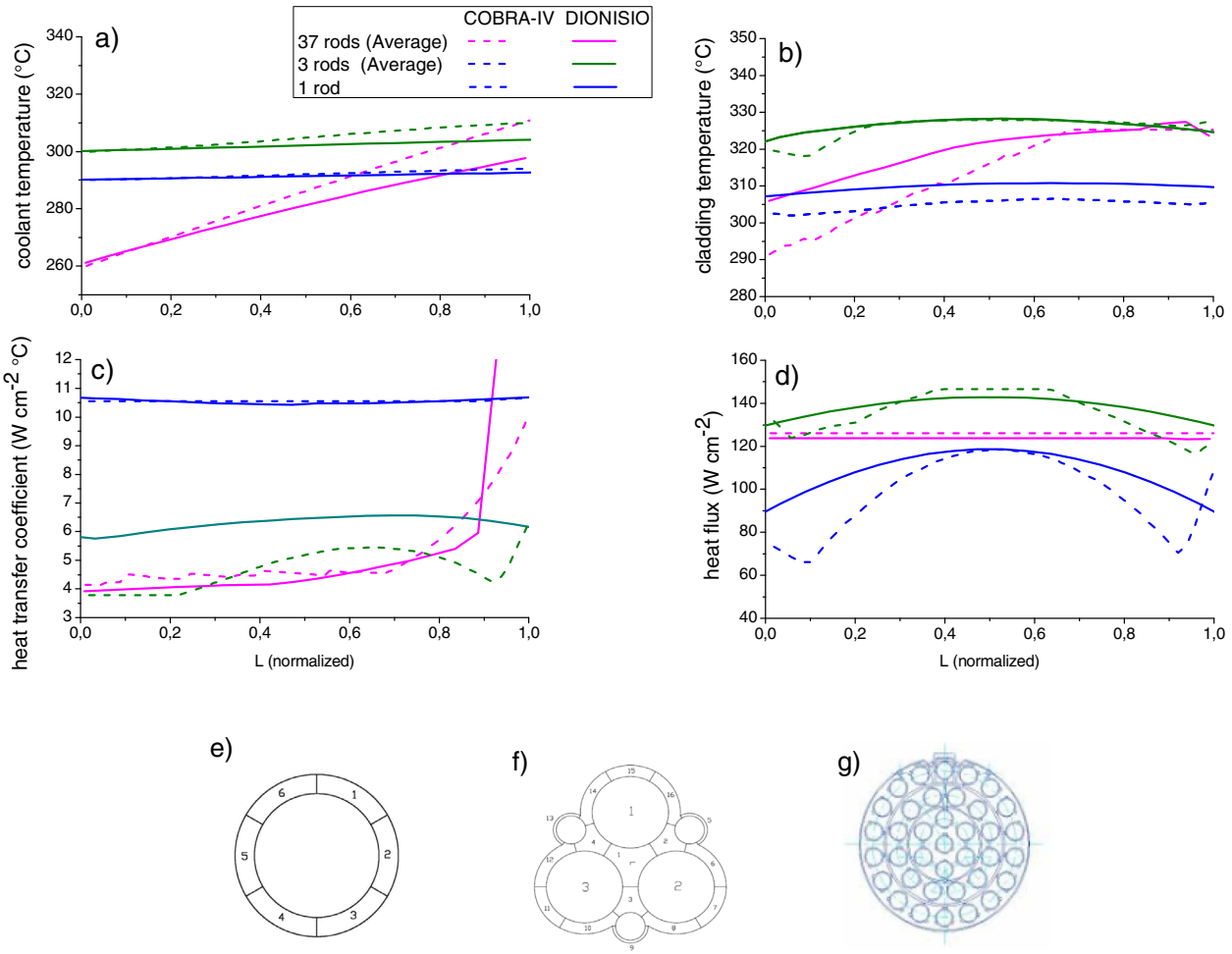

Fig. 6. Comparison between DIONISIO and COBRA-IV of: a) coolant temperature; b) cladding temperature; c) heat transfer coefficient; d) heat flux; for e) a single rod; f) three rods in a channel; g) a fuel bundle of 37 rods.

mocouples were placed at three axial positions in such a way that the temperature in these points was known during the whole experiment.

Fig. 7 shows the linear power and coolant pressure histories along with the records of the three thermocouples. The power history exhibits four constant steps and the pressure history shows six sudden drops followed by recovery periods. As for the temperature, the curves measured with the three thermocouples are superimposed with those calculated at the 20 axial segments into which the rod was divided for the simulation. It is observed that the experimental temperatures fall within the range spread by the predictions, with a very good agreement between them.

The experimental device employed in IFA 650-2 consisted of a loop filled with heavy water initially at high pressure (700 N/cm^2) flowing at a rate of 0.056 kg/s. The device was instrumented with a pressure sensor and four thermocouples located, one of them (TCC1) at the lower part of the rod and the others (TCC2, -3 and -4) at the upper part. To simulate accident conditions the temperature was risen. Cladding ballooning and burst occurred during heat up.

In Fig. 8 the measured and calculated internal rod pressure are shown. The steep internal pressure drop indicates burst occurrence, after which, according to the report of the experiment (Ek, 2005), the He pressure should have dropped to the rig pressure, of about 3 bar. This is the condition assumed in the simulation. The apparent discrepancy with the experimental curve is due to the pressure sensor design, which is not capable of measuring pressures below 56 bars (the value indicated with the dashed line in Fig. 8). The code predicts burst occurrence at t = 110 s while the experimental work reports a value of 99 s. The pressure decrease observed in the experimental curve prior to burst is attributed to the effect of ballooning (Ek, 2005). DIONISIO is not able to reproduce this effect because the mechanical models included in the code assume small strains, which is not the case. A model adequate for large strains is presently under development.

In Fig. 9 the temperatures reached on the external cladding surface as measured with the thermocouples TCC1, TCC2 and TCC3 are plotted. For the simulations the rod is divided into 20 axial segments. The curves plotted in Fig. 9 correspond to those segments that better coincide with the thermocouples location. The instants of ballooning initiation and burst occurrence, measured and predicted, are also shown. The good coincidence between both sets of results can be appreciated. The coolant pressure as determined in the experiment is represented along with the curve fitted in the present work which served as input for DIONISIO. The steep external pressure drop represents the accident initiation (t = 0). The plot also includes the linear power history.

The measured and simulated values of cladding elongation are represented in Fig. 10 as functions of time after blow-down. The experimental curve shows an axial contraction which is associated with the occurrence of ballooning. The contraction stops abruptly and this is interpreted as the instant when burst occurs, 99 s after

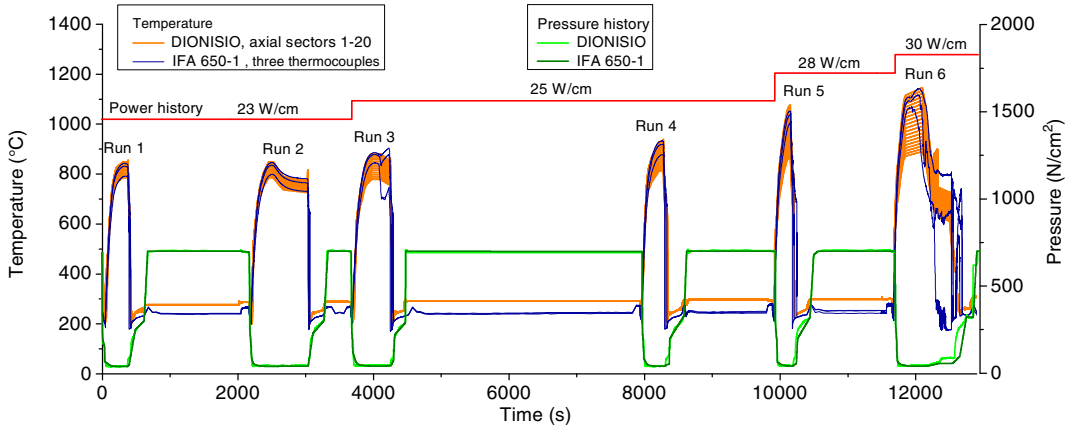

Fig. 7. Comparison of DIONISIO with the IFA 650-1 experiment. Power history in red line; pressure history, experimental curve in dark green, calculated results in light green; temperature evolution, experimental results in blue and simulated in orange. (For interpretation of the references to colour in this figure legend, the reader is referred to the web version of this article.)

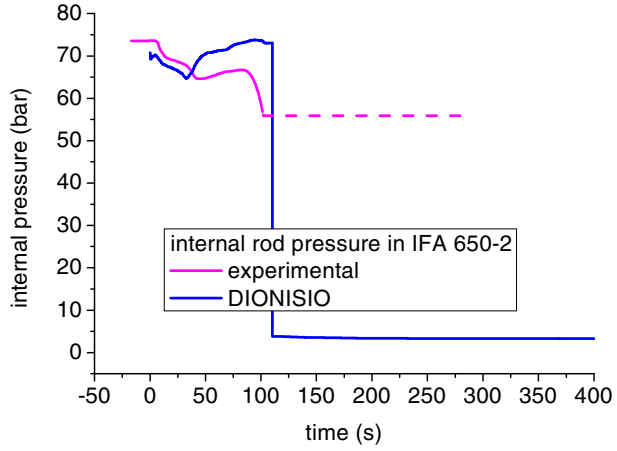

Fig. 8. Comparison between calculated and measured internal rod pressure.

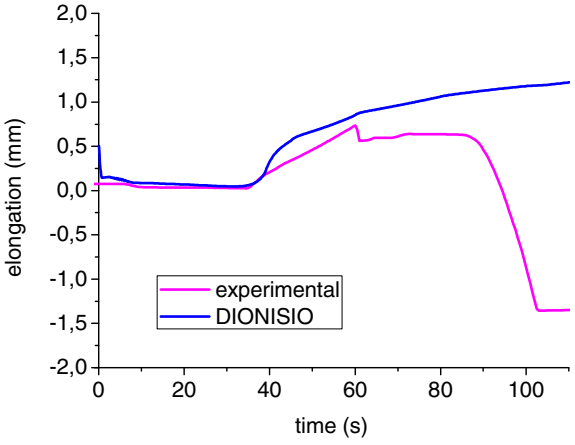

Fig. 10. Comparison between calculated and measured axial cladding elongation in IFA 650-2.

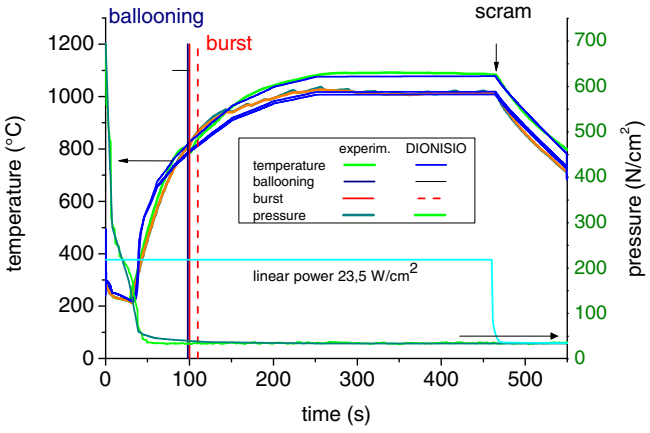

Fig. 9. Comparison between calculated and measured cladding temperature at two axial positions vs. time after accident initiation in IFA 650-2. Predicted and measured ballooning and burst times as well as the scram are also indicated.

blow-down (Ek, 2005). The photographs obtained after experiment conclusion show a major relocation which is surely responsible for the significant rod contraction observed in the final step. This phenomenon implies large deformations and involves the whole rod. For the same reasons as explained in connection with Fig. 8, this is not accounted for in DIONISIO and for this reason both curves depart significantly some 80 s after blow-down. Before that, the agreement between simulation and measurement is quite good.

3.4. Comparison with predictions of ATHLET and RELAP5 for the IAEA-PMK-2 experiments

Several experiments were performed in the PMK-2 facility (in Budapest) between 1984 and 1993. The device is a scaled model of the Paks NPP, designed to extend the data base for VVER-type power plants, to investigate the processes following small and medium size breaks (of 1%–22%) in the primary circuit and also to test the thermal-hydraulic simulation codes in these conditions. The system consists of 19 fuel rods distributed in a hexagon, containing UO_2 pellets in Zry claddings. The experiments were organized by the International Atomic Energy Agency (IAEA) in cooperation with the Atomic Energy Research Institute (AEKI) of the Hungarian Academy of Sciences. These experiments were also aimed at investigating the capability of thermal-hydraulic codes for modeling natural circulation phenomena in these reactors. The results of the experiment and calculations with ATHLET and RELAP-5 are compared (Szabados et al., 1995; Ezsöl et al., 1996).

The computer code ATHLET Mod 1.1 Cycle A was developed by GRS as an advanced best estimate code for the simulation of breaks and transients in PWRs and BWRs including beyond design basis

accidents (Glaeser, 1995). The RELAP5 Mod 3.1 code models the coupled behavior of the reactor coolant system and the core for loss-of-coolant and operational transients (Code Manual and NUREG/CR-5535 INEL-95/0174, 1995).

The DIONISIO code was compared with some of these experiments. In this work the comparison with the fourth experiment of the Standard Problem Exercises (IAEA-SPE-4) is presented. The test, which was performed in April 1993, started from full power and nominal operating conditions: core power 658 kW, primary circuit pressure 12.43 MPa, coolant flow 5.1 kg/s, core inlet temperature 263 °C. During the test one of the thermocouples was located 30 cm below the top of the rod which had a length of 250 cm. To perform the simulation with DIONISIO of the accidental sequence the rod length is divided into 10 axial segments in such a way that the ninth segment coincides quite well with the location of that thermocouple.

In Fig. 11a the coolant flow rate and pressure during the experiment are shown along with the pressure curve fitted as input for DIONISIO. Fig. 11b shows the temperature recorded during the experiment along with the predictions of RELAP5, ATHLET and DIONISIO. The coolant temperature at the bottom of the rod reported in the experiment is compared with the values simulated by DIONISIO corresponding to the first rod segment. The coolant flow drop that starts at about 1000 s is responsible for the steep temperature increase observed in Fig. 11b that ceases when the coolant flow is reestablished. The good agreement with the experimental records reached with DIONISIO can be appreciated.

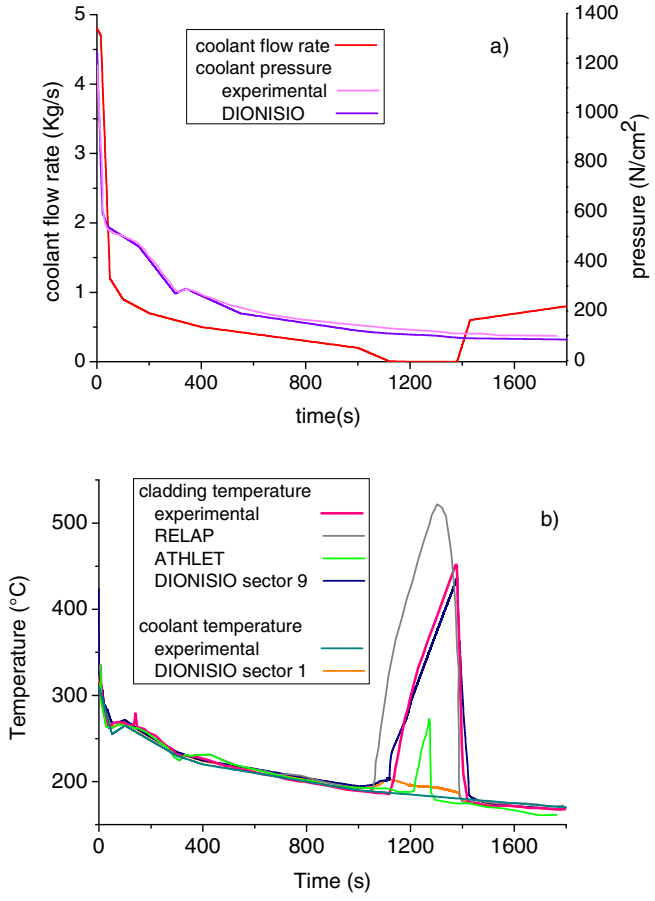

Fig. 11. a) Coolant flow rate and pressure during the experiment; b) Comparison between measured cladding temperature and the predictions of RELAP, ATHLET and DIONISIO, also between the measured coolant temperature at the inlet and the prediction of DIONISIO in sector 1.

4. Discussion and conclusions

The degree of development presently achieved with the thermal-hydraulic model presented here for the cladding-coolant system allows analyzing and quantifying a considerable number of parameters involved in the rod evolution. Accumulated and released heat, temperature distribution in the rod, particularly on its external surface, temperature of the fluid in the cooling channel, vapor mass and volume fractions in the coolant, pressure and coolant flow drop, among others are evaluated not only in normal operation conditions but also in accidental conditions, particularly those described as LOCA events.

The fast variations and the extreme conditions experienced by the fuel rod in this type of accident may cause severe rod damage. Safety reasons indicate the importance of building accurate simulation tools. However, these rapid transients are precisely the cause of some of the more challenging difficulties encountered in the simulations since the general system conditions are definitely far from equilibrium.

The strategy of dividing the rod length into segments, solving the various physical and chemical issues in one representative pellet subjected to the locally averaged conditions of the segment, then extending the results to the whole segment and finally coupling all the segments to reach a description for the entire rod has proved to be effective and quite accurate, particularly in the simulation of normal irradiation conditions. Nevertheless, in accidental conditions, this calculation scheme tends to produce a systematic underestimation of creep and cladding growth. The reason for this relies on the assumption of small strains implied in the model. To overcome this limitation a different scheme valid for large strains is presently under development.

In spite of the approximations implied in the thermal-hydraulic subroutine, the results it produces agree quite well with the available experimental data and with the results of specific codes, thus providing the adequate boundary conditions necessary for the simulation of the fuel rod behavior.

A model to describe the capture and release of Hydrogen in a wide range of scenarios is presently under development and will be incorporated to DIONISIO in the near future as a new subroutine.

Acknowledgemets

The authors wish to acknowledge Mr. Martín Emilio González for the critical revision of the English version of this paper.

This work is performed within the frame of the IAEA Research Contract N°18536 which forms part of the Research Project “Fuel Modeling in Accident Conditions (FUMAC)”.

Mr. Alejandro Soba is also supported by CONICET – Argentina.

References

Soba, A., Denis, A., 2015. DIONISIO 2.0: new version of the code for simulating a whole nuclear fuel rod under extended irradiation. Nucl. Eng. Des. 292, 213–221.

Soba, A., Denis, A., Romero, L., Villarino, E., Sardella, F., 2013. A high burn-up model developed for the DIONISIO code. J. Nucl. Mater. 433 (1–3), 160–166.

Soba, A., Lemes, M., Denis, A., 2015. An empirical formulation to describe the evolution of the high burnup structure. J. Nucl. Mater. 456, 174–181.

Soba, A., Lemes, M., González, M.E., Denis, A., Romero, L., 2014. Simulation of the behaviour of nuclear fuel under high burnup conditions. Ann. Nucl. Energy 70, 147–156.

Rosinger, H.E., 1984. A model to predict the failure of Zircaloy-4 fuel sheathing during postulated LOCA conditions. J. Nucl. Mater. 120 (1), 41–54.

Manngard, T., Jernkvist, L.O., Massih, A., 2011. Evaluation of Loss-of-Coolant Accident Simulation Tests with the Fuel Rod Analysis Code FRAPTRAN-1.4. Quantum Technologies AB. Report TR11-008V1.

Ragheb, M., 2011. Decay Heat Generation in Fission Reactors, Chapter 8. Report University of Illinois at Urbana-Champaign.

MATPRO Version 11, Handbook of Materials Properties for Use in the Analysis of Light Water Reactor Fuel Behavior, 1979. NUREG/CR-0497. TREE-1280.
Delete, G., Charles, M., 1997. Thermal conductivity of fully dense unirradiated UO2: a new formulation from experimental results between 100 C and 2500 C and associated fundamental properties. Water Reactor Fuel Element Modelling at High Burnup and its Experimental Support. IAEA-TECDOC-957, IAEA 203-216.
Fink, J.K., Leibowitz, L., 1995. Thermal conductivity of zirconium. J. Nucl. Mater. 226, 44–50.
Soba, A., Denis, A., 2008. Simulation with DIONISIO 1.0 of thermal and mechanical pellet-cladding interaction in nuclear fuel rods. J. Nucl. Mater. 374, 32–43.
International Agreement Report, 1986. Heat Transfer Processes During Intermediate and Large Break Loss-of-Coolant Accidents (LOCAs). U.S. Nuclear Regulatory Commission.
Mochizuki, H., 2009. Thermal Hydraulics in Nuclear Reactors. International Graduate Course, Tokyo Institute of Technology.
Odar, F., 2001. Assessment of the TRAC-M Codes Using Flecht-Seaset Reflood and Steam Cooling Data. U.S. Nuclear Regulatory Commission.
Todreas, N.E., Kazimi, M.S., 1990. Nuclear Systems I, Thermal Hydraulic Fundamentals. Massachusetts Institute of Technology.
Collier, J.G., Thome, J.R., 1994. Convective Boiling and Condensation. Clarendon Press.
Chen, Y., 2012. An Overview of Heat Transfer Phenomena, Chapter 9: Critical Heat Flux in Subcooled Flow Boiling of Water. http://dx.doi.org/10.5772/52307.
Levy, S., 1967. Forced convection subcooled boiling, prediction of vapor volumetric fraction. Int. J. Heat Mass Transf. 10, 951–965.
FRAPTRAN 1.4: A Computer Code for the Transient Analysis of Oxide Fuel Rods, .
Tong, L.S., Weisman, J., 1966. Thermal Análysis of Pressurized Water Reactors. American Nuclear Society.
Kolev, N.I., 2005. Multiphase Flow Dynamics 2, Thermal and Mechanical Interactions. Springer-Verlag, Berlin Heidelberg.
Ramu, K., Weisman, J., 1977. Transition flow boiling heat transfer to water in a vertical annulus. Nucl. Eng. Des. 40, 285–295.
Cathcart, J.V., Pawel, R.E., McKee, R.A., Druschel, R.E., Yurek, G.J., Campbell, J.J., Jury, S.H., 1977. Zirconium Metal-water Oxidation Kinetics IV. Reaction Rate Studies. ORNL/NUREG-17.
Webb, B.J., 1988. COBRA-IV PC: A Personal Computer Version of COBRA-IV-I for Thermal-Hydraulic Analysis of Rod Bundle Nuclear Fuel Elements and Cores. PNL-6476.
Lestinen, V., Kolstad, E., Wiesenack, W., 2003. LOCA testing at Halden, trial runs in IFA-650. Nuclear Safety Research Conference Washington.
Lestinen, V., 2004. LOCA Testing at Halden, First Experiment IFA-650.1 HWR-762.
Ek, M., 2005. LOCA Testing at Halden; The Second Experiment IFA-650.2, HWR-813.
Szabados, L., Ezsöl, Gy., Perneczky, L., Krepper, E., Prasser, H.M., Schäfer, F., 1995. Two Phase Flow Behavior During a Medium Size Cold Leg LOCA Test on PMK-2 (IAEA SPE-4). KFKI Atomic Energy Research Institute, Budapest, Hungary.
Ezsöl, Gy., Guba, A., Perneczky, L., Krepper, E., Prasser, H.M., Schäfer, F., 1996. Simulation of a Small Cold-leg-Break Experiment at the PMK-2 Test Facility Using the RELAP-5 and ATHLET Codes.
Glaeser, H., 1995. Validation and Uncertainty Analysis of the ATHLET Thermal-Hydraulic Computer Code, Nuclear Society of Slovenia 2nd Regional Meeting. Nuclear Energy in Central Europe, Portoroz, Slovenia.
RELAP5/MOD3 Code Manual, 1995. NUREG/CR-5535 INEL-95/0174 Vol. 5, Rev. 1.